

# Central exclusive production of $\eta$ and $\eta'$ mesons in diffractive proton-proton collisions at the LHC within the tensor-pomeron approach

Piotr Lebiedowicz,<sup>1,\*</sup> Otto Nachtmann,<sup>2,†</sup> and Antoni Szczurek<sup>1,3,‡</sup>

<sup>1</sup>*Institute of Nuclear Physics Polish Academy of Sciences, Radzikowskiego 152, PL-31342 Kraków, Poland*

<sup>2</sup>*Institut für Theoretische Physik, Universität Heidelberg, Philosophenweg 16, D-69120 Heidelberg, Germany*

<sup>3</sup>*Institute of Physics, Faculty of Exact and Technical Sciences, University of Rzeszów, Pigoń 1, PL-35310 Rzeszów, Poland*

We present a study of the central exclusive production (CEP) of  $\eta$  and  $\eta'$ (958) mesons in diffractive proton-proton collisions at high energies. The amplitudes, including pomeron and  $f_{2R}$  reggeon exchanges, are calculated within the tensor-pomeron model. Absorption effects are also taken into account at the amplitude level. We fit some undetermined model parameters (coupling constants and cutoff parameters in form factors) to the WA102 experimental data and then make predictions for the LHC energy  $\sqrt{s} = 13$  TeV. Both, total cross sections and several differential distributions are presented. For  $pp \rightarrow pp\eta$ , we find an upper limit for the total cross section of  $2.5 \mu\text{b}$  for pseudorapidity of the  $\eta$  meson  $|\eta_M| < 1$  and  $5.6 \mu\text{b}$  for  $2 < \eta_M < 5$ . For  $pp \rightarrow pp\eta'$ , we predict the cross section to be in the range of  $0.3\text{--}0.7 \mu\text{b}$  for pseudorapidity of the  $\eta'$  meson  $|\eta_M| < 1$  and  $0.9\text{--}2.1 \mu\text{b}$  for  $2 < \eta_M < 5$ . This opens the possibility to study diffractive production of pseudoscalar mesons in experiments at the LHC. We discuss if there are arguments from SU(3)-flavor symmetry which would forbid pomeron-pomeron fusion giving an  $\eta$  meson. In our opinion such arguments do not exist. We also consider CEP of the pseudoscalars  $\eta$  and  $\eta'$ (958) and the pseudovector meson  $f_1(1285)$  in diffractive proton-proton collisions in a theory with a scalar pomeron. We show that none of these particles can be produced in this way in the scalar-pomeron theory. Thus, experimental observation of any of these particles in the above CEP processes at the LHC would give striking evidence against a scalar character of the pomeron.

## I. INTRODUCTION

Central exclusive production (CEP) of  $\eta$  and  $\eta'$  mesons with  $J^{PC} = 0^{-+}$  in proton-proton collisions has been a subject of both theoretical and experimental studies. Diffractive production of pseudoscalar mesons at high energies can be mediated by the double-pomeron-exchange mechanism [1]. The Born-level amplitudes for  $\eta$  and  $\eta'$  production were derived in [1] in the tensor-pomeron approach [2]. The effective coupling vertices for the fusion of two tensor pomerons into a pseudoscalar meson were derived from the corresponding interaction Lagrangians. Within this framework, there are two independent  $\mathbb{P}\mathbb{P}\eta$  and  $\mathbb{P}\mathbb{P}\eta'$  couplings possible, corresponding to the allowed values of  $(l, S) = (1, 1)$  and  $(3, 3)$ , where  $l$  denotes the orbital angular momentum and  $S$  the total spin of the two tensor pomerons. To be precise,  $l$  and  $S$  refer to the fictitious reaction of two “real” spin 2 pomerons fusing to give  $\eta$  or  $\eta'$ ; see (A.10)–(A.16) and Table 6 of [1]. The covariant couplings of the pomerons to these particles are then constructed accordingly. The corresponding coupling constants were fitted to differential distributions of the WA102 Collaboration [3] at  $\sqrt{s} = 29.1$  GeV and to the total cross sections given in Table 1 of [4]. We cannot exclude the possibility that secondary reggeon exchanges may play an important role in the WA102 energy range; see Sec. 3.2 of [1] and the discussion in [5]. It is found in [1] that for the  $\eta$  meson production the inclusion of additional tensorial contributions of  $f_{2R}\mathbb{P}$ ,  $\mathbb{P}f_{2R}$ , and  $f_{2R}f_{2R}$  to the  $\mathbb{P}\mathbb{P}$  contribution improves the description of experimental differential distributions. Production of  $\eta'$  meson seems to be less affected by contributions from subleading exchanges.

The purpose of our analysis is to provide theoretical predictions for the production of  $\eta$  and  $\eta'$  in the  $pp \rightarrow pp\eta(\eta')$  reactions within the tensor-pomeron approach for experiments at the LHC, where pomeron-pomeron fusion is the dominant production mechanism. In the present work we improve the results given in [1] and extend them to LHC energies. The consideration of adding absorption effects to the Born amplitudes due to proton-proton interactions is an important point of the current analysis. Some of the model parameters can then be estimated by comparing the model results with the WA102 data, as was done for the CEP of  $f_1$  mesons in [5].

It is worth noting that CEP of  $\eta$  and  $\eta'$  mesons was discussed earlier in [6–10]. We believe, however, that pomeron couplings that are essential in the construction of matrix elements for a given type of soft process should be treated as tensor couplings. Some remarks on different views of the pomeron were made in [11]. It was shown there that

\* Piotr.Lebiedowicz@ifj.edu.pl

† O.Nachtmann@thphys.uni-heidelberg.de

‡ Antoni.Szczurek@ifj.edu.pl

only the tensor ansatz for the soft pomeron is compatible with the STAR results from polarized elastic proton-proton scattering [12]. In [13], the authors gave further strong evidence against the hypothesis that the pomeron has vector character. In light of the arguments in these works, we cannot support the conclusions of [14, 15] that the pomeron transforms as a non-conserved vector current as was deduced from the comparison of their model results with data measured by the WA102 Collaboration [16]. In our articles, see for examples Refs. [1, 5, 17–22], we showed that the tensor-pomeron concept for the central production of mesons works quite well in reproducing the data when available.

In [23, 24] the  $pp \rightarrow pp\eta$  process was discussed using the Sakai-Sugimoto model. There, also a comparison of the model with the total cross section measured by the WA102 Collaboration [3] was done. The total cross section calculated in the Sakai-Sugimoto model was found to be about an order of magnitude smaller than the WA102 result. For some related analyses based on the holographic model of QCD see [25]. Finally, we note that in [5] the relation between two different approaches, the tensor-pomeron model and the Sakai-Sugimoto model, for the  $\mathbb{P}\mathbb{P}f_1$  couplings was discussed. By freely adjusting the coupling constants in both models, considering only the pomeron-pomeron fusion mechanism, a reasonable agreement with the WA102 data on CEP of  $f_1$  was obtained. Due to the potential impact of secondary reggeon exchanges at lower energies, where the parameters of our model were fixed, our predictions for the LHC given there should be considered as upper limits of the cross sections.<sup>1</sup>

Experimental studies of processes involving light mesons in the final state at LHC energies would be particularly helpful in order to get a better understanding of various theoretical aspects of these reactions. We will learn, for instance, about pomeron-pomeron-meson couplings, absorption effects, and the role of subleading exchanges. Of particular interest is the transition between the nonperturbative (small meson transverse momenta) and perturbative (large meson transverse momenta) regimes. The perturbative mechanism for CEP of pseudoscalar mesons was considered in [26, 27].

Our paper is organized as follows. In the next section we discuss first the scalar-pomeron case. Then we give analytic expressions for the amplitudes for the  $pp \rightarrow pp\eta(\eta')$  reactions in the tensor-pomeron model. The results of our calculations are presented in Sec. III. Section IV contains our conclusions. In Appendix A we discuss the  $\mathbb{P}f_{2R}\eta(\eta')$  couplings needed for our calculations.

## II. DIFFRACTIVE PRODUCTION OF $\eta$ AND $\eta'(958)$ MESONS IN PROTON-PROTON COLLISIONS

We study central exclusive production of  $\eta$  and  $\eta'(958)$  in proton-proton collisions

$$p(p_a, \lambda_a) + p(p_b, \lambda_b) \rightarrow p(p_1, \lambda_1) + M(k) + p(p_2, \lambda_2), \quad (2.1)$$

where  $p_{a,b}$ ,  $p_{1,2}$  and  $\lambda_{a,b}$ ,  $\lambda_{1,2} = \pm\frac{1}{2}$  denote the four-momenta and helicities of the protons, respectively. The four-momentum of the meson  $M$  ( $\eta$  or  $\eta'(958)$ ) with  $I^G(J^{PC}) = 0^+(0^{-+})$  is denoted by  $k$ .

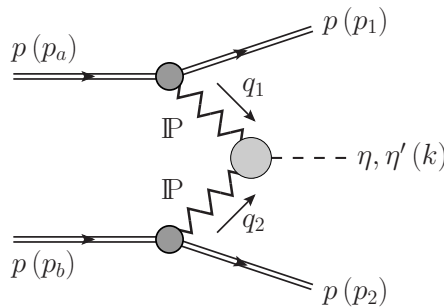
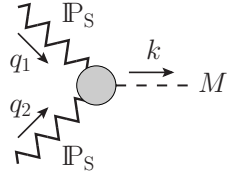


FIG. 1. The Born-level diagram for the reaction (2.1) with double-pomeron exchange (i.e.,  $\mathbb{P}\mathbb{P}$ -fusion mechanism).

We focus here on the  $pp \rightarrow ppM$  processes mediated by double-pomeron exchange, shown at the Born level by the diagram in Fig. 1. Let us first assume that the pomeron has a scalar character replacing  $\mathbb{P}$  by a scalar  $\mathbb{P}_S$  in Fig. 1.

<sup>1</sup> If at the WA102 energies there are important contributions from subleading reggeon-pomeron and reggeon-reggeon fusion terms, the cross sections at LHC energies could be significantly smaller. The reduction could be up to a factor of 4 as estimated in Appendix D of [5] for the CEP of  $f_1(1285)$ .

We are then dealing with the vertex function  $\Gamma^{(\mathbb{P}_S \mathbb{P}_S \rightarrow M)}$  which can only be a function of  $q_1^2$ ,  $q_2^2$ , and  $k^2$ , due to Lorentz invariance:



$$i\Gamma^{(\mathbb{P}_S \mathbb{P}_S \rightarrow M)}(q_1^2, q_2^2, k^2). \quad (2.2)$$

In strong interactions we have parity invariance. For a pseudoscalar meson  $M$  we must have

$$\Gamma^{(\mathbb{P}_S \mathbb{P}_S \rightarrow M)}(q_1'^2, q_2'^2, k'^2) = -\Gamma^{(\mathbb{P}_S \mathbb{P}_S \rightarrow M)}(q_1^2, q_2^2, k^2), \quad (2.3)$$

where

$$\begin{aligned} q_1'^\mu &= \mathcal{P}^\mu_\nu q_1^\nu, & q_2'^\mu &= \mathcal{P}^\mu_\nu q_2^\nu, & k'^\mu &= \mathcal{P}^\mu_\nu k^\nu, \\ (\mathcal{P}^\mu_\nu) &= \text{diag}(1, -1, -1, -1). \end{aligned} \quad (2.4)$$

But we have

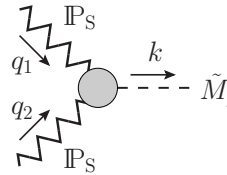
$$q_1'^2 = q_1^2, \quad q_2'^2 = q_2^2, \quad k'^2 = k^2. \quad (2.5)$$

Therefore, we conclude:

$$\Gamma^{(\mathbb{P}_S \mathbb{P}_S \rightarrow M)}(q_1^2, q_2^2, k^2) = 0. \quad (2.6)$$

With a scalar pomeron CEP of a pseudoscalar meson  $M$  with  $I^G(J^{PC}) = 0^+(0^{-+})$  is not possible.

In a similar way we discuss the coupling of an axial-vector meson  $\tilde{M}$  where  $I^G(J^{PC}) = 0^+(1^{++})$  to two scalar pomerons



$$i\Gamma_\mu^{(\mathbb{P}_S \mathbb{P}_S \rightarrow \tilde{M})}(q_1, q_2). \quad (2.7)$$

Here Lorentz invariance requires

$$\Gamma^\mu(\mathbb{P}_S \mathbb{P}_S \rightarrow \tilde{M})(q_1, q_2) = (q_1 + q_2)^\mu A(q_1^2, q_2^2, k^2) + (q_1 - q_2)^\mu B(q_1^2, q_2^2, k^2), \quad (2.8)$$

where  $A(\cdot)$  and  $B(\cdot)$  are invariant functions. Requiring in (2.8) parity invariance leads to

$$\Gamma^\mu(\mathbb{P}_S \mathbb{P}_S \rightarrow \tilde{M})(q_1', q_2') = -\mathcal{P}^\mu_\nu \Gamma^\nu(\mathbb{P}_S \mathbb{P}_S \rightarrow \tilde{M})(q_1, q_2), \quad (2.9)$$

which implies

$$A(q_1^2, q_2^2, k^2) = B(q_1^2, q_2^2, k^2) = 0. \quad (2.10)$$

CEP of an axial-vector meson  $\tilde{M}$  is not possible with a scalar pomeron. A prominent axial-vector meson is the  $f_1(1285)$ .

In our paper we treat the reactions (2.1) in the tensor-pomeron approach as introduced in [2]. The pomeron ( $\mathbb{P}$ ) with the charge conjugation  $C = +1$  is described as effective rank-two symmetric tensor exchange.

The kinematic variables are

$$\begin{aligned}
q_1 &= p_a - p_1, & q_2 &= p_b - p_2, & k &= q_1 + q_2, \\
t_1 &= q_1^2, & t_2 &= q_2^2, \\
u_1 &= (p_a - k)^2 = (p_1 - q_2)^2, \\
u_2 &= (p_b - k)^2 = (p_2 - q_1)^2, \\
s &= (p_a + p_b)^2 = (p_1 + p_2 + k)^2, \\
s_1 &= (p_a + q_2)^2 = (p_1 + k)^2, \\
s_2 &= (p_b + q_1)^2 = (p_2 + k)^2, \\
v_1 &= \frac{1}{4}(s_1 - u_1) = \frac{1}{4}(p_a + p_1, q_2 + k) = \frac{1}{2}(p_a + p_1, k), \\
v_2 &= \frac{1}{4}(s_2 - u_2) = \frac{1}{4}(p_b + p_2, q_1 + k) = \frac{1}{2}(p_b + p_2, k).
\end{aligned} \tag{2.11}$$

For a detailed discussion of the kinematics see e.g. Appendix D of [1].

The amplitude for the  $\mathbb{P}\mathbb{P}$  fusion to a pseudoscalar particle or resonance  $M$  reads

$$\mathcal{M}_{pp \rightarrow ppM}^{(\mathbb{P}\mathbb{P})} = \mathcal{M}_{pp \rightarrow ppM}^{\text{Born}} + \mathcal{M}_{pp \rightarrow ppM}^{pp\text{-rescattering}}. \tag{2.12}$$

The second term represents the  $pp$ -rescattering corrections to the first (Born) term.

The Born amplitude is given by

$$\begin{aligned}
\mathcal{M}_{\lambda_a \lambda_b \rightarrow \lambda_1 \lambda_2 M}^{\text{Born}} &= (-i) \bar{u}(p_1, \lambda_1) i\Gamma^{(\mathbb{P}pp)} \mu_1 \nu_1(p_1, p_a) u(p_a, \lambda_a) \\
&\times i\Delta_{\mu_1 \nu_1, \alpha_1 \beta_1}^{(\mathbb{P})}(2\nu_1, t_1) i\Gamma^{(\mathbb{P}PM)} \alpha_1 \beta_1, \alpha_2 \beta_2(q_1, q_2) i\Delta_{\alpha_2 \beta_2, \mu_2 \nu_2}^{(\mathbb{P})}(2\nu_2, t_2) \\
&\times \bar{u}(p_2, \lambda_2) i\Gamma^{(\mathbb{P}pp)} \mu_2 \nu_2(p_2, p_b) u(p_b, \lambda_b).
\end{aligned} \tag{2.13}$$

The corresponding expressions for the effective proton vertex function and propagator for the tensor-pomeron exchange are as follows (see Sec. 3 of [2])

$$i\Gamma_{\mu\nu}^{(\mathbb{P}pp)}(p', p) = -i3\beta_{\mathbb{P}NN}F_1(t) \left\{ \frac{1}{2} [\gamma_\mu(p' + p)_\nu + \gamma_\nu(p' + p)_\mu] - \frac{1}{4}g_{\mu\nu}(\not{p}' + \not{p}) \right\}, \tag{2.14}$$

$$i\Delta_{\mu\nu, \kappa\lambda}^{(\mathbb{P})}(2\nu_{1,2}, t) = \frac{1}{8\nu_{1,2}} \left( g_{\mu\kappa}g_{\nu\lambda} + g_{\mu\lambda}g_{\nu\kappa} - \frac{1}{2}g_{\mu\nu}g_{\kappa\lambda} \right) (-i2\nu_{1,2}\alpha_{\mathbb{P}}')^{\alpha_{\mathbb{P}}(t)-1}, \tag{2.15}$$

where  $t = (p' - p)^2$  and  $\beta_{\mathbb{P}NN} = 1.87 \text{ GeV}^{-1}$ . For simplicity we use for the pomeron-proton coupling the electromagnetic Dirac form factor  $F_1(t)$  of the proton. The pomeron trajectory  $\alpha_{\mathbb{P}}(t)$  is assumed to be of standard form

$$\alpha_{\mathbb{P}}(t) = \alpha_{\mathbb{P}}(0) + \alpha_{\mathbb{P}}' t, \quad \alpha_{\mathbb{P}}(0) = 1 + \epsilon_{\mathbb{P}} = 1.0808, \quad \alpha_{\mathbb{P}}' = 0.25 \text{ GeV}^{-2}. \tag{2.16}$$

In (2.13) and (2.15) we use  $2\nu_1$  and  $2\nu_2$  instead of  $s_1$  and  $s_2$ , respectively, as variables in the pomeron propagators; cf. (3.10) of [2]. It is well known that in Regge theory  $2\nu$  is the variable which appears naturally because of its crossing properties; see for instance chapter 6.4 of [28] and chapter 6 of [2]. At high energies and small  $|t|$ , the kinematic regime considered in [2], we have  $2\nu \rightarrow s$ . We have checked numerically that the use of  $2\nu_{1,2}$  instead of  $s_{1,2}$  is significant at the WA102 energy ( $\sqrt{s} = 29.1 \text{ GeV}$ ) and leads to an increase of cross section of about 30–40%, depending on the model parameters (i.e., on the share of exchange contributions) used. At LHC energies, we can use with very good accuracy the approximations  $2\nu_1 \approx s_1$  and  $2\nu_2 \approx s_2$ , especially for the midrapidity production of the mesons.

The  $\mathbb{P}\mathbb{P}M$  coupling was discussed in Sec. 2.2 of [1]. The resulting  $\mathbb{P}\mathbb{P}M$  vertex, including a form factor, is given as

follows [see (2.4) and (2.6) of [1]]

$$i\Gamma_{\mu\nu,\kappa\lambda}^{(\text{PPM})}(q_1, q_2) = \left( i\Gamma_{\mu\nu,\kappa\lambda}'^{(\text{PPM})}(q_1, q_2) |_{\text{bare}} + i\Gamma_{\mu\nu,\kappa\lambda}''^{(\text{PPM})}(q_1, q_2) |_{\text{bare}} \right) F(q_1^2, q_2^2), \quad (2.17)$$

$$i\Gamma_{\mu\nu,\kappa\lambda}'^{(\text{PPM})}(q_1, q_2) |_{\text{bare}} = i \frac{g_{\text{PPM}}'}{2M_0} (g_{\mu\kappa}\varepsilon_{\nu\lambda\rho\sigma} + g_{\nu\kappa}\varepsilon_{\mu\lambda\rho\sigma} + g_{\mu\lambda}\varepsilon_{\nu\kappa\rho\sigma} + g_{\nu\lambda}\varepsilon_{\mu\kappa\rho\sigma}) (q_1 - q_2)^\rho (q_1 + q_2)^\sigma, \quad (2.18)$$

$$i\Gamma_{\mu\nu,\kappa\lambda}''^{(\text{PPM})}(q_1, q_2) |_{\text{bare}} = i \frac{g_{\text{PPM}}''}{M_0^3} \left\{ \varepsilon_{\nu\lambda\rho\sigma} [q_{1\kappa}q_{2\mu} - (q_1 \cdot q_2)g_{\mu\kappa}] + \varepsilon_{\mu\lambda\rho\sigma} [q_{1\kappa}q_{2\nu} - (q_1 \cdot q_2)g_{\nu\kappa}] \right. \\ \left. + \varepsilon_{\nu\kappa\rho\sigma} [q_{1\lambda}q_{2\mu} - (q_1 \cdot q_2)g_{\mu\lambda}] + \varepsilon_{\mu\kappa\rho\sigma} [q_{1\lambda}q_{2\nu} - (q_1 \cdot q_2)g_{\nu\lambda}] \right\} (q_1 - q_2)^\rho (q_1 + q_2)^\sigma. \quad (2.19)$$

In (2.18) and (2.19)  $M_0 \equiv 1 \text{ GeV}$  and  $g_{\text{PPM}}'$ ,  $g_{\text{PPM}}''$  are dimensionless coupling constants that should be fitted to experimental data. The  $\Gamma_{\mu\nu,\kappa\lambda}'$  and  $\Gamma_{\mu\nu,\kappa\lambda}''$  bare vertices correspond to  $(l, S) = (1, 1)$  and  $(3, 3)$ , respectively, as derived from the corresponding coupling Lagrangians (2.3) and (2.5) in [1].

The form factor in the central vertex is parametrized as

$$F(t_1, t_2) = \frac{1}{1 - t_1/\Lambda_0^2} \frac{1}{1 - t_2/\Lambda_0^2}, \quad \Lambda_0^2 = 0.5 \text{ GeV}^2. \quad (2.20)$$

Alternatively, we use the exponential form given by

$$F(t_1, t_2) = \exp\left(\frac{t_1 + t_2}{\Lambda_E^2}\right), \quad (2.21)$$

where  $\Lambda_E$  is the cutoff parameter fitted to the experimental data as we will show below in Sec. III A.

The amplitude representing absorption corrections due to the proton-proton interactions can be written as

$$\mathcal{M}_{pp \rightarrow ppM}^{pp\text{-rescattering}}(s, \mathbf{p}_{t,1}, \mathbf{p}_{t,2}) = \frac{i}{8\pi^2 s} \int d^2 \mathbf{l}_t \mathcal{M}_{pp \rightarrow pp}(s, -\mathbf{l}_t^2) \mathcal{M}_{pp \rightarrow ppM}^{\text{Born}}(s, \tilde{\mathbf{p}}_{t,1}, \tilde{\mathbf{p}}_{t,2}). \quad (2.22)$$

Here, in the overall center-of-mass (c.m.) system,  $\mathbf{p}_{t,1}$  and  $\mathbf{p}_{t,2}$  are the transverse components of the momenta of the outgoing protons and  $\mathbf{l}_t$  is the transverse momentum carried around the pomeron loop.  $\mathcal{M}_{pp \rightarrow ppM}^{\text{Born}}$  is the Born amplitude given by (2.13) with  $\tilde{\mathbf{p}}_{t,1} = \mathbf{p}_{t,1} - \mathbf{l}_t$  and  $\tilde{\mathbf{p}}_{t,2} = \mathbf{p}_{t,2} + \mathbf{l}_t$ .  $\mathcal{M}_{pp \rightarrow pp}$  is the elastic  $pp$  scattering amplitude given by (6.28) in [2] for large  $s$  and with the momentum transfer  $t = -\mathbf{l}_t^2$ . In practice we work with the amplitudes in the high-energy approximation, where  $s$ -channel-helicity conservation of the protons holds.

In addition to the  $\mathbb{P}$ P fusion, we also consider the  $\mathbb{P}f_{2\mathbb{R}}$ ,  $f_{2\mathbb{R}}\mathbb{P}$ , and  $f_{2\mathbb{R}}f_{2\mathbb{R}}$  exchanges. Since both  $\mathbb{P}$  and  $f_{2\mathbb{R}}$  are described as tensor exchanges, the additional amplitudes,  $\mathcal{M}^{(\mathbb{P}f_{2\mathbb{R}})}$ ,  $\mathcal{M}^{(f_{2\mathbb{R}}\mathbb{P})}$ , and  $\mathcal{M}^{(f_{2\mathbb{R}}f_{2\mathbb{R}})}$ , are treated similarly to (2.12)–(2.19). The effective  $f_{2\mathbb{R}}$ -proton vertex function and the  $f_{2\mathbb{R}}$  propagator are given in [2] by Eqs. (3.49) and (3.12), respectively. The important differences there are in the magnitude of the coupling constant and the parametrization of the trajectory:

$$3\beta_{\mathbb{P}NN} \rightarrow \frac{g_{f_{2\mathbb{R}}PP}}{M_0}, \quad g_{f_{2\mathbb{R}}PP} = 11.04, \quad (2.23)$$

$$\alpha_{\mathbb{P}}(t) \rightarrow \alpha_{\mathbb{R}_+}(t) = \alpha_{\mathbb{R}_+}(0) + \alpha'_{\mathbb{R}_+} t, \quad \alpha_{\mathbb{R}_+}(0) = 0.5475, \quad \alpha'_{\mathbb{R}_+} = 0.9 \text{ GeV}^{-2}. \quad (2.24)$$

We use  $2\nu_{1,2}$  instead of  $s_{1,2}$  as variables in the  $f_{2\mathbb{R}}$  propagators.

Note that in the reaction  $\mathbb{P}f_{2\mathbb{R}} \rightarrow M$  two *different* objects fuse to give the pseudoscalar meson  $M$ . But with the methods of Appendix A of [1] we show in Appendix A that also here we have only the two couplings corresponding to  $(l, S) = (1, 1)$  and  $(3, 3)$ . Therefore, the bare vertices  $\mathbb{P}f_{2\mathbb{R}}M$  and  $f_{2\mathbb{R}}f_{2\mathbb{R}}M$  are as the  $\mathbb{P}PM$  ones in (2.18) and (2.19), but with different coupling constants  $(g_{\mathbb{P}f_{2\mathbb{R}}M}', g_{\mathbb{P}f_{2\mathbb{R}}M}'')$  and  $(g_{f_{2\mathbb{R}}f_{2\mathbb{R}}M}', g_{f_{2\mathbb{R}}f_{2\mathbb{R}}M}'')$ , respectively. These coupling constants will be roughly fitted to existing central production data from the WA102 experiment; see Table I of Sec. III A below. We made the simplifying assumption that the form factor  $F(t_1, t_2)$  is of the same type for all couplings.

### III. RESULTS

In this section we present our results for the reactions  $pp \rightarrow pp\eta$  and  $pp \rightarrow pp\eta'$  at c.m. energy of  $\sqrt{s} = 29.1$  GeV together with the WA102 experimental data and our predictions for LHC experiments at  $\sqrt{s} = 13$  TeV.

#### A. Comparison with the WA102 data

According to Ref. [4] the WA102 experimental cross sections for central production of  $\eta$  and  $\eta'(958)$  mesons in  $pp$  collisions at  $\sqrt{s} = 29.1$  GeV are

$$\eta : \sigma_{\text{exp.}} = (3859 \pm 368) \text{ nb}, \quad (3.1)$$

$$\eta'(958) : \sigma_{\text{exp.}} = (1717 \pm 184) \text{ nb}. \quad (3.2)$$

In [3, 4] also the distributions in  $\phi_{pp}$ ,  $t$ ,  $dP_t$ , and  $x_{F,M}$  for the  $\eta$  and  $\eta'$  production were presented. Here,  $t$  is the four-momentum transfer squared from one of the proton vertices [we have  $t = t_1$  or  $t_2$ ; cf. (2.11)],  $\phi_{pp}$  is the azimuthal angle between the transverse momentum vectors  $\mathbf{p}_{t,1}$  and  $\mathbf{p}_{t,2}$  of the outgoing protons in the overall c.m. system,  $dP_t$  (the so-called “glueball-filter variable” [29, 30]) is defined as

$$dP_t = \mathbf{q}_{t,1} - \mathbf{q}_{t,2} = \mathbf{p}_{t,2} - \mathbf{p}_{t,1}, \quad dP_t = |d\mathbf{P}_t|, \quad (3.3)$$

and the Feynman- $x$  variable is defined as  $x_{F,M} = 2p_{z,M}/\sqrt{s}$  with  $p_{z,M}$  the longitudinal momentum of the meson in this c.m. system.

In Fig. 2 we show the results for the  $pp \rightarrow pp\eta'$  reaction at  $\sqrt{s} = 29.1$  GeV. The WA102 data points from [3] have been normalized to the mean value of the total cross section (3.2). In Fits 1, 2, and 3 we consider  $\mathbb{P}\mathbb{P}$  plus  $f_{2R}f_{2R}$  fusion processes. By comparing the theoretical results and the WA102 distributions we fixed the parameters in the  $\mathbb{P}\mathbb{P}\eta'$  and  $f_{2R}f_{2R}\eta'$  vertices. We also present the results when the contribution of the exchanges  $\mathbb{P}f_{2R}$  plus  $f_{2R}\mathbb{P}$  are included in the calculation. These correspond to Fits 4, 5, and 6. The numerical values of the parameters used in the calculations are collected in Table I. We can see from Table I how the choice of the type of the form factor  $F(t_1, t_2)$  in (2.17) and the cutoff parameter affect the strength of the different coupling constants.

TABLE I. Parameters of the model determined from the fit to the WA102 data at  $\sqrt{s} = 29.1$  GeV and the resulting cross sections with absorption effects are presented. In the last column we present the ratio of the cross sections with ( $\sigma_{\text{abs}}$ ) and without ( $\sigma_{\text{Born}}$ ) absorption effects,  $S^2 = \sigma_{\text{abs}}/\sigma_{\text{Born}}$ .

Meson $M$	Fit	$\mathcal{G}'_{\mathbb{P}\mathbb{P}M}$	$\mathcal{G}''_{\mathbb{P}\mathbb{P}M}$	$\mathcal{G}'_{\mathbb{P}f_{2R}M}$	$\mathcal{G}''_{\mathbb{P}f_{2R}M}$	$\mathcal{G}'_{f_{2R}f_{2R}M}$	$\mathcal{G}''_{f_{2R}f_{2R}M}$	Cutoff parameter	$\sigma_{\text{abs}} (\mu\text{b})$	$S^2$
$\eta'(958)$	1	2.7	1.2	0	0	-10.0	0	$\Lambda_0^2 = 0.5 \text{ GeV}^2$	1.74	0.60
	2	2.7	1.2	0	0	-10.0	0	$\Lambda_E = 0.8 \text{ GeV}$	1.74	0.63
	3	2.05	1.2	0	0	-10.0	0	$\Lambda_E = 1.0 \text{ GeV}$	1.75	0.60
	4	1.6	1.2	1.8	0	-10.0	0	$\Lambda_E = 1.0 \text{ GeV}$	1.72	0.62
	5	1.4	1.4	2.3	0	-10.0	0	$\Lambda_E = 1.0 \text{ GeV}$	1.75	0.65
	6	1.4	1.4	2.5	0	10.0	0	$\Lambda_E = 1.0 \text{ GeV}$	1.75	0.63
	7	1.4	1.4	1.3	0	-25.0	0	$\Lambda_E = 1.0 \text{ GeV}$	1.75	0.66
	8	1.4	1.4	2.15	0	25.0	0	$\Lambda_E = 1.0 \text{ GeV}$	1.74	0.65
$\eta$	A	1.8	1.8	0	0	10.0	0	$\Lambda_E = 1.0 \text{ GeV}$	3.73	0.66
	B	1.0	1.0	1.1	3.0	4.0	0	$\Lambda_E = 1.0 \text{ GeV}$	3.55	0.73
	C	1.0	1.0	1.1	3.0	-4.0	0	$\Lambda_E = 1.0 \text{ GeV}$	3.64	0.67
	D	1.0	1.0	1.7	4.0	-4.0	0	$\Lambda_E = 0.8 \text{ GeV}$	3.66	0.73

For a deeper insight, we calculate the percentage share of different exchanges to the total cross section for the  $pp \rightarrow pp\eta'$  reaction at  $\sqrt{s} = 29.1$  GeV. In Fit 5,  $\mathbb{P}\mathbb{P}$  accounts for 39%,  $\mathbb{P}f_{2R} + f_{2R}\mathbb{P}$  for 28%, and  $f_{2R}f_{2R}$  for only 3%. There is a large interference effect between these terms in the amplitude of about 30% with respect to the total cross section.

For the CEP of the  $\eta'$  meson, the ratio of the cross sections measured by the WA102 experiment at  $\sqrt{s} = 29.1$  GeV to that measured by the WA76 experiment at  $\sqrt{s} = 12.7$  GeV was determined in [16] to be

$$\frac{\sigma(\sqrt{s} = 29.1 \text{ GeV})}{\sigma(\sqrt{s} = 12.7 \text{ GeV})} = 0.72 \pm 0.16. \quad (3.4)$$

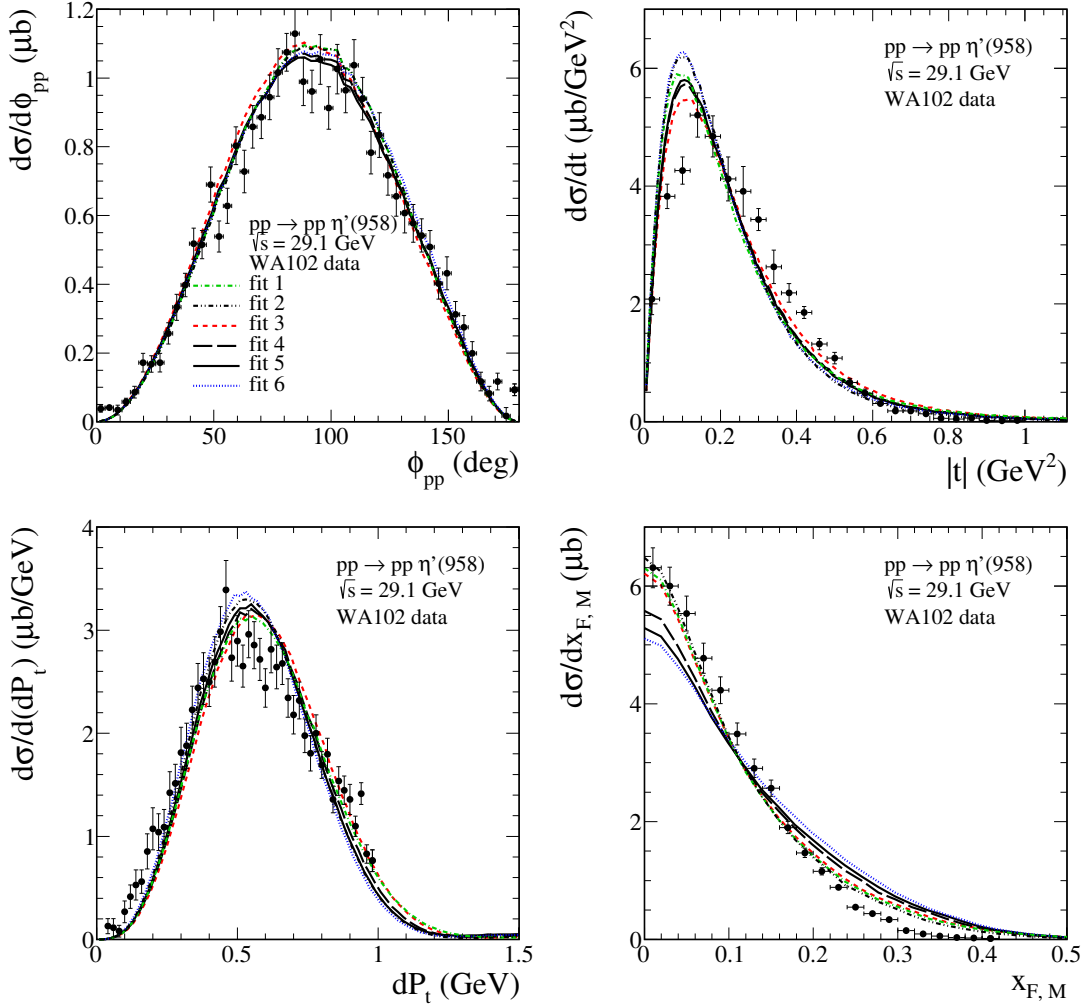


FIG. 2. Fits to the WA102 data [3] for  $\eta'$  meson production at  $\sqrt{s} = 29.1$  GeV. The absorption effects are included in the calculations. For the line description see Table I.

The ratios we obtained for the parameter sets 1–6 from Table I are as follows 1.46, 1.47, 1.31, 1.29, 1.29, 1.19. In the calculations, we assumed a rather large value of the coupling constant  $g'_{f_{2R}f_{2R}\eta'}$ , and despite this we do not reproduce the experimental result (3.4). The discrepancy may indicate a certain role of other processes, e.g.  $\omega\omega$ ,  $\rho^0\rho^0$ ,  $\omega_R\omega_R$ , and  $\rho_R\rho_R$  exchanges. To obtain a value of 0.7 for the ratio (3.4), we need  $g'_{f_{2R}f_{2R}\eta'} \sim \pm 25.0$  as in sets 7 and 8 of Table I. Then, this parameter should be regarded as effective because it replaces the contribution of other (non-included) processes. With the parameter set 7 and for  $\sqrt{s} = 29.1$  GeV, the  $\mathbb{P}\mathbb{P}$  contribution accounts for 39%,  $\mathbb{P}f_{2R} + f_{2R}\mathbb{P}$  for 9%, and  $f_{2R}f_{2R}$  for 22% of the total cross section  $\sigma(\sqrt{s} = 29.1 \text{ GeV}) = 1.75 \mu\text{b}$ . For  $\sqrt{s} = 12.7$  GeV we obtain respectively 13%, 6%, and 61% of  $\sigma(\sqrt{s} = 12.7 \text{ GeV}) = 2.50 \mu\text{b}$ . As  $\sqrt{s}$  increases from 12.7 GeV to 29.1 GeV, the cross section of the  $f_{2R}f_{2R}$  exchange decreases by a factor of four, it increases slightly for the  $\mathbb{P}f_{2R} + f_{2R}\mathbb{P}$  fusion processes and increases by a factor of 2.1 for the  $\mathbb{P}\mathbb{P}$  fusion.

In Fig. 3 we show our fit results and the WA102 data for the  $pp \rightarrow pp\eta$  reaction at  $\sqrt{s} = 29.1$  GeV. The WA102 data points from [3] have been normalized to the mean value of the total cross section (3.1). For the description of  $\eta$  production the  $\mathbb{P}\mathbb{P}$ ,  $\mathbb{P}f_{2R}$ ,  $f_{2R}\mathbb{P}$ , and  $f_{2R}f_{2R}$  exchanges in the amplitude are included. In the calculations we use four sets of parameters corresponding to Fits A–D in Table I. In Set A, we assume that the  $\mathbb{P}\mathbb{P}$ -exchange contribution is more important than in others. In Fit C,  $\mathbb{P}\mathbb{P}$  represents 40%,  $\mathbb{P}f_{2R} + f_{2R}\mathbb{P}$  accounts for 32%, and  $f_{2R}f_{2R}$  for 5%. In Fit D we have 25%, 48%, and 4%, respectively.

In Fig. 4 we show the two-dimensional distributions in  $(\sqrt{2v_1}, \sqrt{2v_2})$ . The results for set A (left panel) and set C (right panel) are presented. We can see how these variables are correlated in the  $\sqrt{2v_1}$ - $\sqrt{2v_2}$  plane. We find that the main contribution comes from the region where  $\sqrt{2v_1}\sqrt{2v_2} \approx 20 \text{ GeV}^2$ . This is not far from the naive expectation

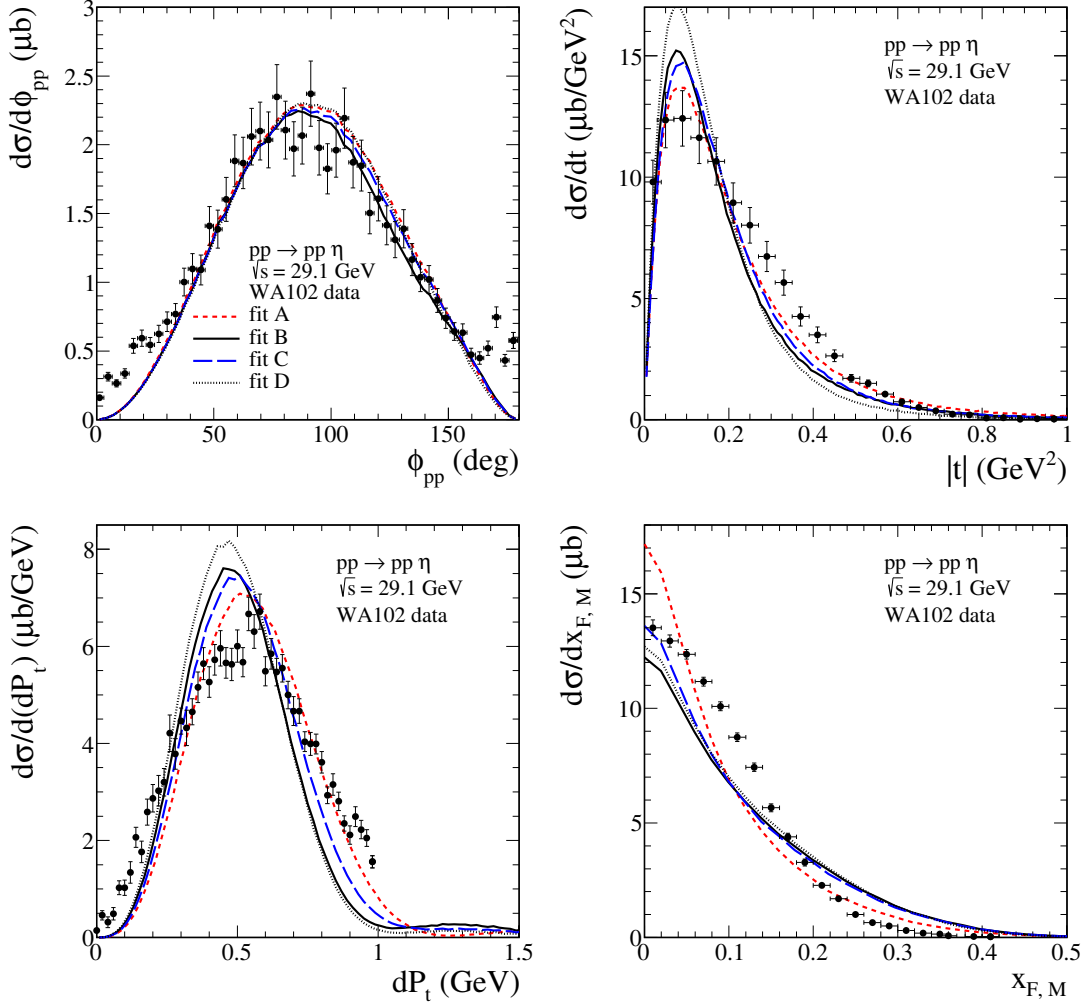


FIG. 3. Fits to the WA102 data [3] for  $\eta$  meson production at  $\sqrt{s} = 29.1$  GeV. The absorption effects are included in the calculations. For the line description see Table I.

$\sqrt{2v_1}\sqrt{2v_2} \approx \sqrt{s_1 s_2} \approx m_\eta \sqrt{s} \approx 16 \text{ GeV}^2$ ; see (D.17) of [1].

Now we summarize our analysis for the  $pp \rightarrow pp\eta'$  and  $pp \rightarrow pp\eta$  reactions of this section. We have shown that double-pomeron exchange, with suitable  $\mathbb{P}\mathbb{P}\eta'$ ,  $\mathbb{P}f_{2R}\mathbb{P}\eta' + f_{2R}\mathbb{P}\eta'$ , and  $f_{2R}f_{2R}\eta'$  couplings, can give a reasonable description of the WA102 data at  $\sqrt{s} = 29.1$  GeV. We have seen that in order to reproduce the shape of the  $\phi_{pp}$  distribution with a maximum at  $\phi_{pp} = \pi/2$ , the two  $(l, S) = (1, 1)$  and  $(3, 3)$  couplings are needed with  $g''_{\mathbb{P}\mathbb{P}M}/g'_{\mathbb{P}\mathbb{P}M} \simeq 0.5$ . The dominant contribution to the cross section is from the coupling  $(l, S) = (1, 1)$ . If there are important contributions with subleading  $f_{2R}$ -pomeron and  $f_{2R}$ - $f_{2R}$  exchanges, the  $\mathbb{P}\mathbb{P}\eta'$  couplings could be significantly smaller. In this case, our fits 5 and 6 suggest that  $g''_{\mathbb{P}\mathbb{P}M}/g'_{\mathbb{P}\mathbb{P}M} \simeq 1.0$ . For the  $pp \rightarrow pp\eta$  reaction, we have found that the contributions of secondary exchanges are also significant. In all cases the interference terms between the different contributions in the amplitudes play an important role.

### B. Comment on the $\mathbb{P}\mathbb{P}\eta$ and $\mathbb{P}\mathbb{P}\eta'$ couplings obtained in the Sakai-Sugimoto model

In [23, 24] the following structure for the  $\mathbb{P}\mathbb{P}M$  vertex (without a form-factor function and using our notation) appears

$$i\Gamma_{\mu\nu,\kappa\lambda}^{\text{CS}}(q_1, q_2) = 2i[(\varkappa_a - \varkappa_b(q_1 \cdot q_2))g_{\nu\lambda} + \varkappa_b q_{1\lambda}q_{2\nu}] \varepsilon_{\mu\kappa\rho\sigma} q_1^\rho q_2^\sigma. \quad (3.5)$$



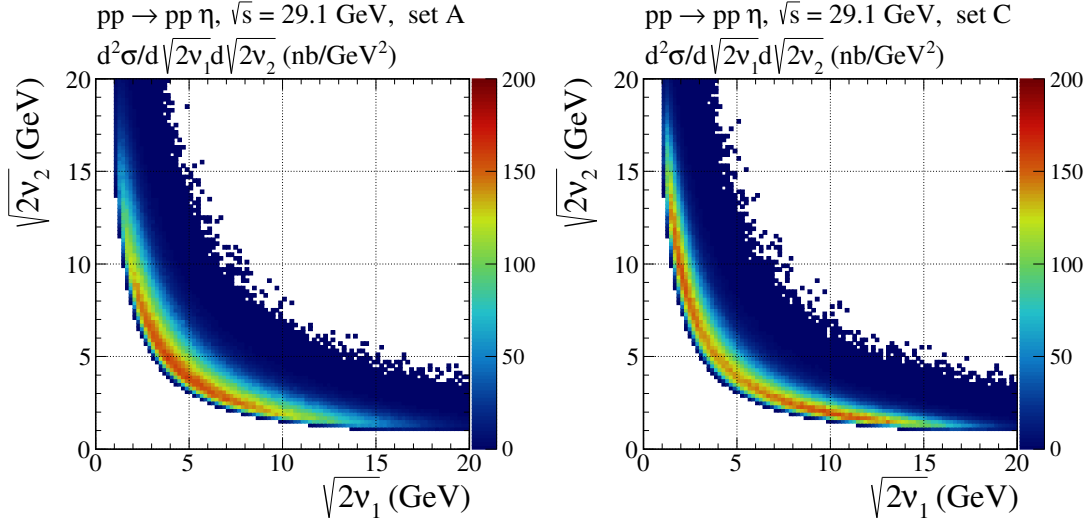


FIG. 4. The two-dimensional distributions in  $(\sqrt{2v_1}, \sqrt{2v_2})$  for the  $pp \rightarrow pp\eta$  reaction calculated for  $\sqrt{s} = 29.1$  GeV. The results for set A (left panel) and set C (right panel) are shown.

The values of the coupling constants  $(\kappa_a, \kappa_b) = (0.084 \text{ GeV}^{-1}, 0.182 \text{ GeV}^{-3})$  were determined using the Sakai-Sugimoto model in Sec. IV of [23]. Note that in Table I of [24] smaller values for  $(\kappa_a, \kappa_b) = (0.0222 \text{ GeV}^{-1}, 0.0482 \text{ GeV}^{-3})$  are quoted. Nevertheless, the ratio is predicted to be  $\kappa_b/\kappa_a \simeq 2.17 \text{ GeV}^{-2}$ . The structure of the PPM coupling is universal (model independent), but the specific values of the coupling constants depend on the details of the Sakai-Sugimoto model. There is evidence that the Sakai-Sugimoto model may underestimate the values of the relevant coupling constants [23, 24].

It is easy to see that the equivalence relation

$$\Gamma' + \Gamma'' = \Gamma^{\text{CS}} \quad (3.6)$$

between the ‘bare’ vertices (2.18), (2.19) and (3.5) holds if the respective coupling parameters satisfy the following conditions

$$g'_{\text{PPM}} = \kappa_a \frac{M_0}{2}, \quad g''_{\text{PPM}} = \kappa_b \frac{M_0^3}{4}. \quad (3.7)$$

In Sec. III A we fix the coupling parameters  $g'_{\text{PPM}}$  and  $g''_{\text{PPM}}$  from the comparison of the tensor-pomeron model with the WA102 experimental data. From (3.7) we have

$$\frac{g''_{\text{PPM}}}{g'_{\text{PPM}}} = \frac{M_0^2}{2} \frac{\kappa_b}{\kappa_a}, \quad (3.8)$$

and using the values of  $\kappa_a$  and  $\kappa_b$  from [23, 24] we get  $g''_{\text{PPM}}/g'_{\text{PPM}} \approx 1.1$ . This is in good agreement with our findings from Fit 5 and Fit 6 for the  $\eta'$  production as far as this ratio is concerned. But the magnitude of coupling constants predicted in [23, 24] is much smaller than what we find in the tensor-pomeron approach from the comparison with the WA102 data; see Table I.

It may be that the WA102 energy is too low to draw firm conclusions on the  $\text{PP}\eta'$  couplings due to very important contributions from reggeon-pomeron and reggeon-reggeon exchanges. The study of CEP of  $\eta'$  at LHC energies should answer this question since there certainly PIP fusion is the dominant mechanism.

### C. Predictions for the LHC experiments

First we present our results for  $pp \rightarrow pp\eta'$  for the LHC energy  $\sqrt{s} = 13$  TeV where subleading reggeon contributions should be negligible, at least, for the midrapidity region. We consider parameter sets 1–6 corresponding to fits 1–6 as determined from the comparison with the WA102 data (see Fig 2 and Table I).

Figure 5 shows our results including a cut on the pseudorapidity of the  $\eta'$  meson  $|\eta_M| < 1.0$ . We see that  $\eta'$  mesons are predominantly produced with the transverse momentum  $p_{t,M} \simeq 0.5$  GeV and with momentum transfers between the protons of the order  $p_{t,p} \sim \sqrt{|t_{1,2}|} \simeq 0.35$  GeV. In all cases the absorption effects are included. The main effect of absorption is a reduction of cross sections by about 60% (see the values of  $S^2$  in Table II below). It also modifies the differential distributions because their shapes depend on the kinematics of the outgoing protons. For instance, the maximum of the  $\phi_{pp}$  distribution is shifted from 90 degrees towards smaller angles of about 70 degrees.

In Fig. 6 we show the rapidity ( $y_M$ ) and pseudorapidity ( $\eta_M$ ) distributions of the  $\eta'$  meson. The minimum in the pseudorapidity distribution at  $\eta_M = 0$  can be understood as a kinematic effect; see Appendix D of [1]. We can see that the pomeron-reggeon and reggeon-pomeron exchanges are separated and contribute at backward and forward meson rapidity, respectively. The interference of these terms with the dominant  $\mathbb{P}\mathbb{P}$  exchange produces enhancements of the cross section at  $y_M \gtrsim 3$ . This effect of secondary reggeon exchanges could be tested by the LHCb Collaboration.

Figure 6 clearly shows that  $\mathbb{P}f_{2R}$  fusion effects, which could be responsible for a rather large fraction of the cross sections at the WA102 energy, will be negligible at the LHC energy. Thus, LHC experiments will settle the question of the magnitudes of the  $\mathbb{P}\mathbb{P}\eta'$  couplings. The comparison of the fits to the WA102 and the LHC data will be an important issue since we will learn from it the magnitude of the subleading exchange contributions.

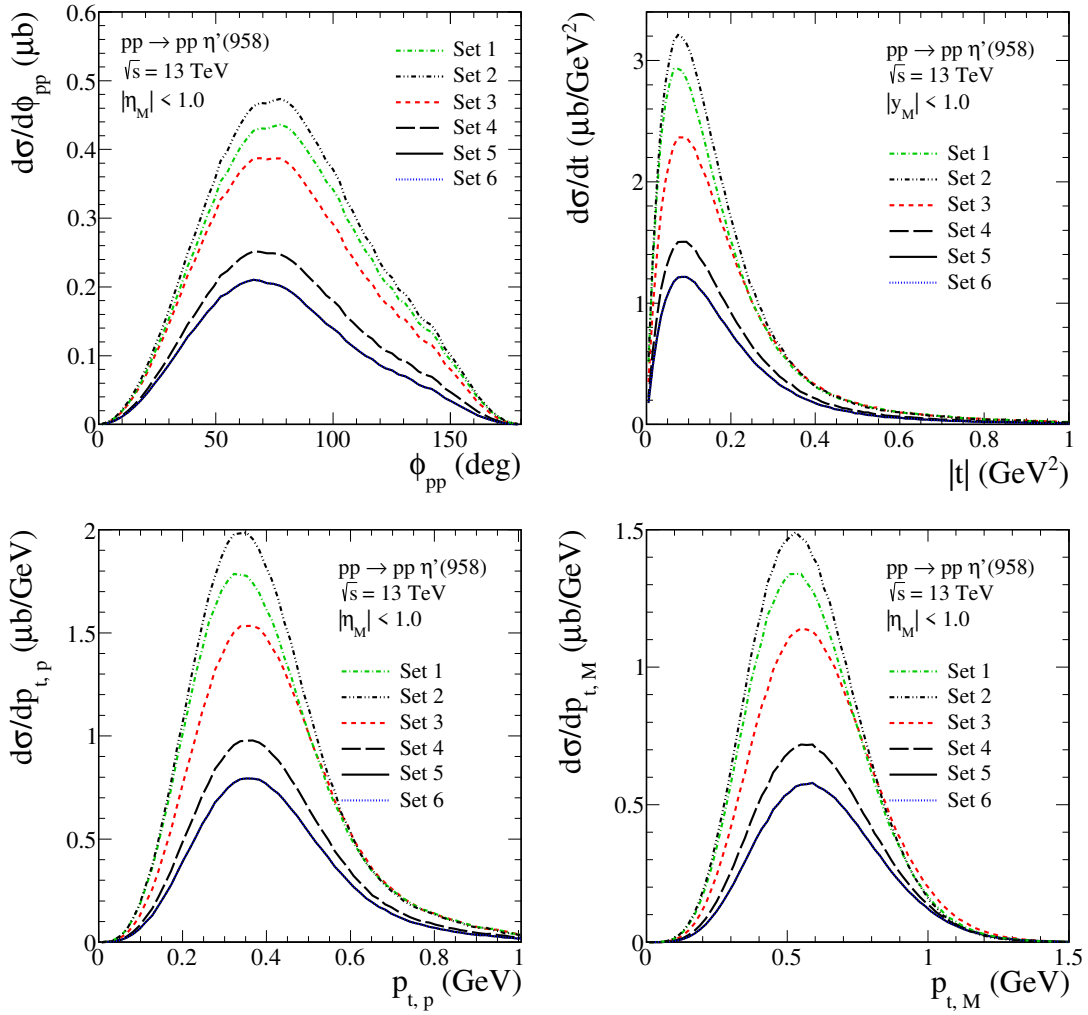


FIG. 5. The differential cross sections for the  $pp \rightarrow pp\eta'$  reaction calculated at  $\sqrt{s} = 13$  TeV and for  $|\eta_M| < 1.0$ . Here  $\eta_M$  is the pseudorapidity of the  $\eta'$  meson in the overall c.m. system. The results for the parameter sets 1–6 (corresponding to fit 1–6 in Table I) are shown. The results for sets 5 and 6 are practically identical due to the small  $f_{2R}f_{2R}$ -exchange contribution at the LHC kinematics. The absorption effects are included in the calculations.

In Fig. 7 we show our predictions for the  $pp \rightarrow pp\eta$  reaction for the parameter sets A–D given in Table I. We see

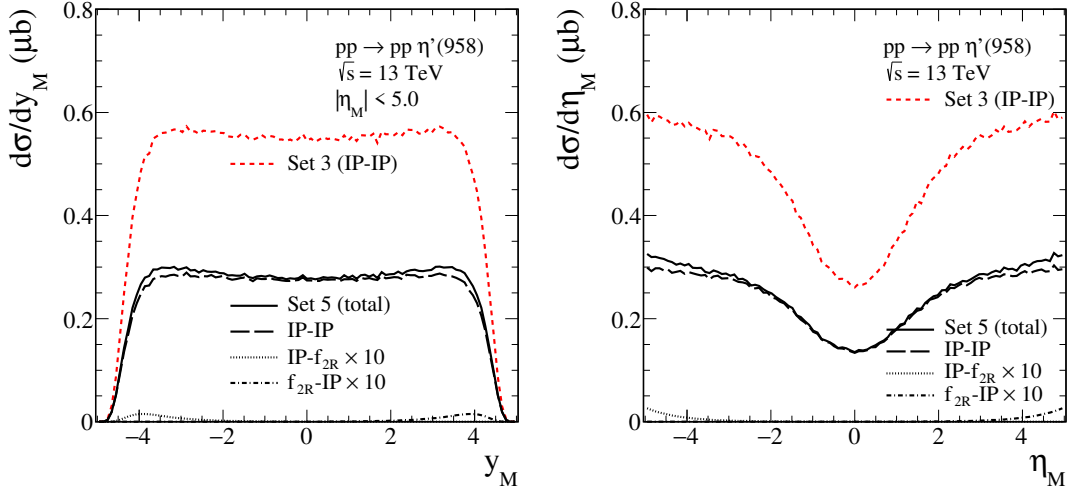


FIG. 6. The distributions in rapidity ( $y_M$ ) and in pseudorapidity ( $\eta_M$ ) of the  $\eta'$  meson calculated for  $\sqrt{s} = 13$  TeV. The results for the parameter set 3 and 5 are shown. The  $\mathbb{P}f_{2R}$  and  $f_{2R}\mathbb{P}$  contributions (in the case of set 5) are increased by a factor of 10 for visualization purposes. The absorption effects are included in the calculations.

from Fig. 3 and Table I that at the WA102 energy we have fit A to CEP of the  $\eta$  meson where the  $\mathbb{P}\mathbb{P}\eta$  couplings are larger compared to fits B–D. Correspondingly, fit A gives the largest cross sections for the LHC energy in Fig. 7. The decision on the true magnitudes of the  $\mathbb{P}\mathbb{P}\eta$  and the subleading couplings will again be given by the LHC experiments, comparing the LHC data with the WA102 ones.

Figure 8 shows the distributions in  $(\sqrt{2\nu_1}, \sqrt{2\nu_2})$  for the  $pp \rightarrow pp\eta$  reaction. Calculations were done for two parameter sets, A and C. For the LHC kinematics, we have basically  $\sqrt{2\nu_1} = \sqrt{s_1}$  and  $\sqrt{2\nu_2} = \sqrt{s_2}$ . From  $s_1 s_2 \approx m_\eta^2 s$  we get  $\sqrt{2\nu_1}\sqrt{2\nu_2} \approx m_\eta \sqrt{s} = 7.1 \times 10^3 \text{ GeV}^2$ . On the other hand we find from Fig. 8 the main contribution to the cross section for  $\sqrt{2\nu_1}\sqrt{2\nu_2} \approx 9.0 \times 10^3 \text{ GeV}^2$ , not far from the above value. It is important to bear in mind that the energy variables  $\nu_1$  and  $\nu_2$  are correlated, as demonstrated in the figure.

In Table II we have collected cross sections in  $\mu\text{b}$  for the reactions  $pp \rightarrow pp\eta'$  and  $pp \rightarrow pp\eta$  for  $\sqrt{s} = 13$  TeV and for some kinematical cuts on the pseudorapidity of the mesons. We must emphasize that our predictions for CEP of  $\eta'$  and  $\eta$  based on parameter sets 1–3 and set A, respectively, (obtained assuming significant double-pomeron exchange at the WA102 energy  $\sqrt{s} = 29.1$  GeV) should be considered as upper limits of the cross sections. For sets 4–6, the cross section is smaller by a factor of about 2. For the CEP of the  $\eta$  meson, one can see a larger difference in the final results. We can see from comparing the last columns of Tables I and II that the absorption effects are more important at the LHC than at the WA102 energy, leading to a sizable reduction of the cross sections.

Let us finally comment on experimental signatures for our reactions  $pp \rightarrow pp\eta$  and  $pp \rightarrow pp\eta'$ . One of the most prominent decay modes of the  $\eta$  meson is  $\pi^+\pi^-\pi^0$  with the branching fraction  $\mathcal{BR}(\eta \rightarrow \pi^+\pi^-\pi^0) = (23.02 \pm 0.25)\%$  [31]. The final state  $\pi^+\pi^-\pi^0$  is also the main decay mode of the  $\omega$  meson. Recall that in the case of  $pp \rightarrow pp\omega$  at LHC energy, the photoproduction (photon-pomeron fusion processes) mechanism competes with the  $\omega$ -strahlung mechanism; see e.g. [32]. From Fig. 10 of [32] we can see that at midrapidities  $|y_\omega| \lesssim 2$  the photoproduction mechanism dominates over the  $\omega$ -strahlung one. The cross section for photoproduction  $d\sigma(pp \rightarrow pp\omega)/dy_\omega$  is estimated to be  $\sim 0.1 \mu\text{b}$  in the range  $0 < y_\omega < 5$ . Furthermore, experimental observation of a sharp increase of the cross section when going to large  $y_\omega$  would be a clear signature of the  $\omega$ -strahlung production. In our opinion, the measurement of the relative contributions of the mesons  $\eta$  and  $\omega$  in the same system  $\pi^+\pi^-\pi^0$  would provide very valuable information for comparing with model predictions. Such results could be obtained by the ALICE and LHCb Collaborations in experiments when the leading protons are not detected and instead only rapidity-gap conditions are checked experimentally. The channel where the  $\eta'(958)$  resonance is to be observed is  $\pi^+\pi^-\eta$ , and this channel is also prominent for the  $f_1(1285)$  decay. Here we predict much larger cross section for CEP of  $f_1(1285)$  via the  $\mathbb{P}\mathbb{P}$ -fusion process (see Table III of [5]) than for the  $\eta'$ . It should be kept in mind, however, that the theoretical results are sensitive to kinematics, i.e. depend on experimental cuts, as well as on the type of the  $\mathbb{P}\mathbb{P}\eta'$  and  $\mathbb{P}\mathbb{P}f_1$  couplings used in the calculation. Clearly, all these topics deserve careful analyses, but they go beyond the scope of the present paper.

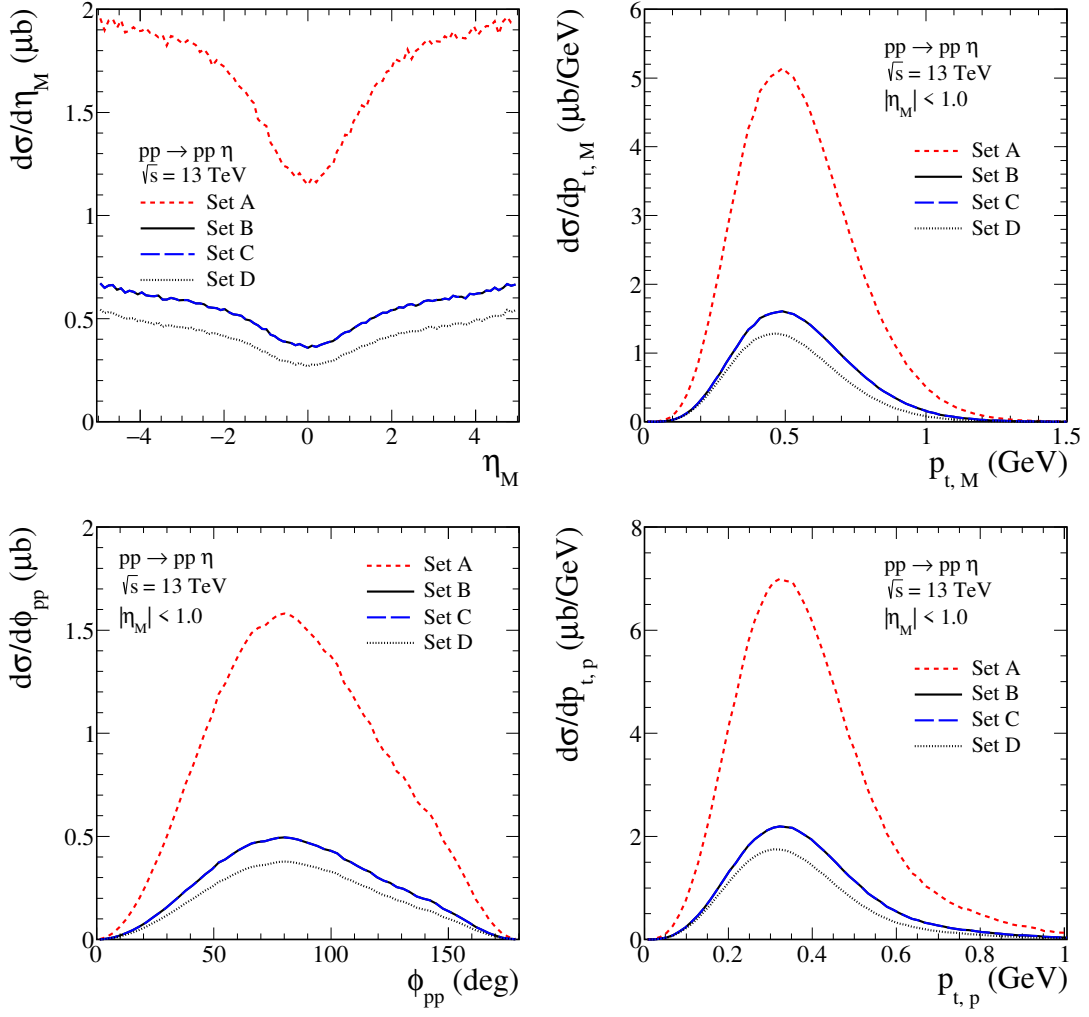


FIG. 7. The differential cross sections for the  $pp \rightarrow pp\eta$  reaction calculated at  $\sqrt{s} = 13$  TeV with cut on  $|\eta_M| < 1.0$ . The results correspond to the parameter sets A–D from Table I. The results for sets B and C are practically identical due to the small  $f_{2R}f_{2R}$ -exchange contribution at the LHC kinematics. The absorption effects are included in the calculations.

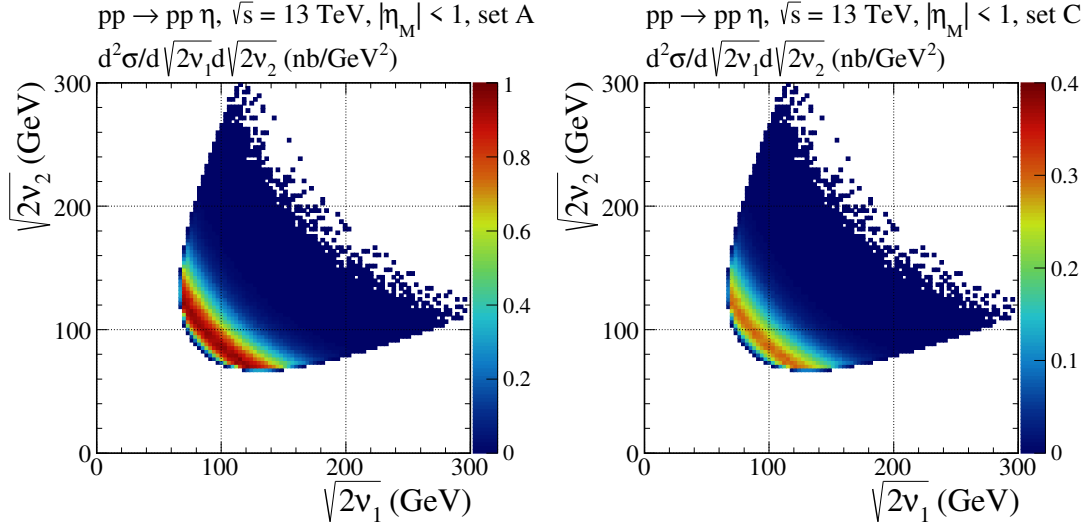


FIG. 8. The distributions in  $(\sqrt{2v_1}, \sqrt{2v_2})$  for the  $pp \rightarrow pp\eta$  reaction calculated for  $\sqrt{s} = 13$  TeV and with cut on  $|\eta_M| < 1$ . The results for set A (left panel) and set C (right panel) are shown.

TABLE II. The integrated cross sections in  $\mu b$  for CEP of  $\eta$  and  $\eta'$  in  $pp$  collisions for  $\sqrt{s} = 13$  TeV for some kinematical cuts on the pseudorapidity of the mesons. The results with absorption effects are presented. In the calculations, we used the parameter sets corresponding to the fits 1–6 for  $\eta'$  and to the fits A–D for  $\eta$  from Table I.

Meson $M$	Cuts	Parameter set	$\sigma_{\text{abs}} (\mu b)$	$S^2$
$\eta' (958)$	$ \eta_M  < 1.0$	1	0.66	0.40
		2	0.72	0.42
		3	0.59	0.39
		4	0.37	0.40
		5	0.30	0.42
		6	0.31	0.42
	$2.0 < \eta_M < 5.0$	1	1.94	0.40
		2	2.09	0.42
		3	1.67	0.39
		4	1.08	0.40
		5	0.88	0.42
		6	0.88	0.42
$\eta$	$ \eta_M  < 1.0$	A	2.51	0.42
		B	0.78	0.42
		C	0.78	0.42
		D	0.59	0.46
	$2.0 < \eta_M < 5.0$	A	5.58	0.42
		B	1.81	0.43
		C	1.81	0.43
		D	1.42	0.46

#### IV. CONCLUSIONS

In this paper we have discussed central exclusive production (CEP) of  $\eta$  and  $\eta'$  mesons in diffractive proton-proton collisions. We have first shown that in a theory where the pomeron couples like a scalar none of the particles  $\eta$ ,  $\eta'$ , and  $f_1(1285)$  can be produced by pomeron-pomeron fusion in CEP. Therefore, observation of CEP of any of these particles at the LHC will be a striking evidence against a scalar character of the pomeron.

We have then discussed in detail, using the tensor-pomeron model,  $\eta$  and  $\eta'$  CEP at the WA102 energy  $\sqrt{s} = 29.1$  GeV and at the LHC energy  $\sqrt{s} = 13$  TeV. We considered the  $\mathbb{P}\mathbb{P}$ , the  $\mathbb{P}f_{2\mathbb{R}} + f_{2\mathbb{R}}\mathbb{P}$ , and the  $f_{2\mathbb{R}}f_{2\mathbb{R}}$  fusion processes giving  $\eta$  and  $\eta'$ . At the low WA102 energy our fits to the data did not give us a clear indication of the relative size of the  $\mathbb{P}\mathbb{P}$ ,  $\mathbb{P}f_{2\mathbb{R}} + f_{2\mathbb{R}}\mathbb{P}$ , and  $f_{2\mathbb{R}}f_{2\mathbb{R}}$  contributions. We have shown that in contrast to this experiments at the LHC should be able to give us precise numbers for the  $\mathbb{P}\mathbb{P}\eta$  and  $\mathbb{P}\mathbb{P}\eta'$  coupling parameters.

Finally we discuss the coupling of two pomerons to the  $\eta$  meson from the point of view of  $SU(3)_F$ -flavor symmetry. If  $SU(3)_F$  was an exact symmetry of QCD the  $\eta$  meson would be a pure  $SU(3)_F$  octet state, the pomeron a pure  $SU(3)_F$  singlet gluonic object and consequently the coupling  $\mathbb{P}\mathbb{P}\eta$  would be zero. But  $SU(3)_F$  is badly broken. There is octet-singlet mixing and the physical  $\eta$  contains both octet and singlet components; see Chapter 15.3 of [31] for a review. Also, there is the possibility of a purely gluonic part in the wave function of the  $\eta$ ; see for instance [33–35]. A direct observation of  $SU(3)_F$  symmetry breaking in the pomeron-meson-meson coupling is provided by the comparison of  $\pi p$  and  $K p$  total cross sections which are, for instance, shown in Figs. 3.1 and 3.2 of [36]. From a fit to these cross sections the pomeron parts are found to be

$$\begin{aligned}\sigma(\pi p)|_{\mathbb{P}} &= 13.63 (sM_0^{-2})^{\epsilon_{\mathbb{P}}}, \\ \sigma(K p)|_{\mathbb{P}} &= 11.93 (sM_0^{-2})^{\epsilon_{\mathbb{P}}}, \\ M_0 &= 1 \text{ GeV}, \quad \epsilon_{\mathbb{P}} = 0.0808.\end{aligned}\tag{4.1}$$

This gives direct evidence for  $SU(3)_F$  breaking in the pomeron-meson-meson coupling. But this can be understood quantitatively in the calculations based on the functional-integral approach to soft high-energy hadron-hadron scattering introduced in [37]; see [38] and Chapter 8 of [36] for reviews. There, hadron-hadron scattering is calculated from the correlation function of lightlike Wegner-Wilson loops representing the hadrons. The results depend, of course, on the transverse size of the loops. This model gives a dependence of the pomeron part of the total cross sections on the hadron radii  $R_h$  divided by  $R_p$ . See Fig. 8.11 of [36] where this is shown for  $\sigma(hp)|_{\mathbb{P}}$  with  $h = p, \pi, K$ , and  $J/\psi$ . In this approach, the size of the strings between the quark and the antiquark in the meson determines the coupling to the pomeron. The quark and antiquark at the endpoints of the string determine the  $SU(3)_F$  assignment of the meson but not directly its coupling to the pomeron. We are looking forward to the measurements of CEP of  $\eta$  and  $\eta'$  mesons at the LHC. These will tell us if in the  $\mathbb{P}\mathbb{P}\eta$  and  $\mathbb{P}\mathbb{P}\eta'$  couplings the string extensions or the flavor quantum numbers at the string endpoints of the mesons are the relevant parameters. A comparatively large  $\mathbb{P}\mathbb{P}\eta$  coupling, as we advocate in our present paper, would be support for the former possibility.

#### ACKNOWLEDGMENTS

The authors would like to thank C. Ewerz, R. McNulty, and R. Schicker for useful discussions. The work of A.S. was partially supported by the Centre for Innovation and Transfer of Natural Sciences and Engineering Knowledge in Rzeszów (Poland).

#### Appendix A: The pomeron- $f_{2\mathbb{R}}$ -pseudoscalar-meson coupling

Here we discuss the couplings  $\mathbb{P}f_{2\mathbb{R}}M$  where  $M$  denotes a pseudoscalar meson. We proceed as in Appendix A of [1]. We consider first the fictitious reaction of a “real pomeron” of spin 2 and a “real  $f_{2\mathbb{R}}$  reggeon” of spin 2 giving the meson  $M$ . Using the notation as in (A.10) of [1] we have in the rest system of  $M$

$$\begin{aligned}\mathbb{P}(k, 2, m_1) + f_{2\mathbb{R}}(-k, 2, m_2) &\rightarrow M(J, J_z), \\ J = 0, \quad J_z = 0, \quad m_{1,2} &\in \{-2, \dots, 2\}.\end{aligned}\tag{A1}$$

Here  $k$  is the momentum,  $J$  the total angular momentum of  $M$ , and  $m_1, m_2$ , and  $J_z$  the  $z$ -components of the angular momenta. We combine the spins of  $\mathbb{P}$  and  $f_{2\mathbb{R}}$  to the total spin

$$S = 0, 1, 2, 3, 4.\tag{A2}$$

Then we combine  $S$  with the angular momentum  $l = 0, 1, 2, \dots$  to give us  $J$ , the total spin of the system. The parity of the state, obtained in complete analogy to (A.11)–(A.13) and (A.15), (A.16), of [1]

$$|l, S; J, J_z\rangle \quad (\text{A3})$$

is then  $(-1)^l$ . Clearly, for  $S$  from (A2) we can get  $J = 0$  only for the following combinations  $(l, S)$  shown in Table III. We get only the combinations  $(l, S) = (1, 1)$  and  $(3, 3)$  which give us a pseudoscalar state.

TABLE III. Values of orbital angular momentum  $l$  and total spin  $S$  which can lead in (A1) to a state with total spin  $J = 0$ .  $P$  is the parity of this state.

$l$	$S$	$J$	$P$
0	0	0	+
1	1	0	−
2	2	0	+
3	3	0	−
4	4	0	+

Now we construct the coupling Lagrangians corresponding to these couplings. For  $(l, S) = (1, 1)$  we set as in (2.3) of [1] with  $\tilde{\chi}_M(x)$  the pseudoscalar meson field

$$\begin{aligned} \mathcal{L}'_{\mathbb{P}f_{2\mathbb{R}}M}(x) &= -\frac{4}{M_0} g'_{\mathbb{P}f_{2\mathbb{R}}M} [\partial_\rho \mathbb{P}_{\mu\nu}(x)] [\partial_\sigma f_{2\mathbb{R}\kappa\lambda}(x)] g^{\mu\kappa} \varepsilon^{\nu\lambda\rho\sigma} \tilde{\chi}_M(x) \\ &= -\frac{2}{M_0} g'_{\mathbb{P}f_{2\mathbb{R}}M} \left\{ [\partial_\rho \mathbb{P}_{\mu\nu}(x)] [\partial_\sigma f_{2\mathbb{R}\kappa\lambda}(x)] g^{\mu\kappa} \varepsilon^{\nu\lambda\rho\sigma} + [\partial_\rho f_{2\mathbb{R}\mu\nu}(x)] [\partial_\sigma \mathbb{P}_{\kappa\lambda}(x)] g^{\mu\kappa} \varepsilon^{\nu\lambda\rho\sigma} \right\} \tilde{\chi}_M(x). \end{aligned} \quad (\text{A4})$$

Here  $\mathbb{P}_{\mu\nu}(x)$  and  $f_{2\mathbb{R}\mu\nu}(x)$  are the effective pomeron and  $f_{2\mathbb{R}}$ -reggeon field operators, respectively. For the  $(l, S) = (3, 3)$  coupling Lagrangian we set as in (2.5) of [1]

$$\begin{aligned} \mathcal{L}''_{\mathbb{P}f_{2\mathbb{R}}M}(x) &= -\frac{2g''_{\mathbb{P}f_{2\mathbb{R}}M}}{M_0^3} \varepsilon^{\mu_1\mu_2\nu_1\nu_2} (\partial_{\mu_1} \tilde{\chi}_M(x)) \left[ (\partial_{\mu_3} \mathbb{P}_{\mu_4\nu_1}(x) - \partial_{\mu_4} \mathbb{P}_{\mu_3\nu_1}(x)) \overset{\leftrightarrow}{\partial}_{\mu_2} (\partial^{\mu_3} f_{2\mathbb{R}}^{\mu_4}{}_{\nu_2}(x) - \partial^{\mu_4} f_{2\mathbb{R}}^{\mu_3}{}_{\nu_2}(x)) \right] \\ &= -\frac{g''_{\mathbb{P}f_{2\mathbb{R}}M}}{M_0^3} \varepsilon^{\mu_1\mu_2\nu_1\nu_2} (\partial_{\mu_1} \tilde{\chi}_M(x)) \left[ (\partial_{\mu_3} \mathbb{P}_{\mu_4\nu_1}(x) - \partial_{\mu_4} \mathbb{P}_{\mu_3\nu_1}(x)) \overset{\leftrightarrow}{\partial}_{\mu_2} (\partial^{\mu_3} f_{2\mathbb{R}}^{\mu_4}{}_{\nu_2}(x) - \partial^{\mu_4} f_{2\mathbb{R}}^{\mu_3}{}_{\nu_2}(x)) \right. \\ &\quad \left. + (\partial_{\mu_3} f_{2\mathbb{R}\mu_4\nu_1}(x) - \partial_{\mu_4} f_{2\mathbb{R}\mu_3\nu_1}(x)) \overset{\leftrightarrow}{\partial}_{\mu_2} (\partial^{\mu_3} \mathbb{P}^{\mu_4}{}_{\nu_2}(x) - \partial^{\mu_4} \mathbb{P}^{\mu_3}{}_{\nu_2}(x)) \right]. \end{aligned} \quad (\text{A5})$$

From (A4) and (A5) we get the bare vertex functions  $\Gamma_{\mu\nu,\kappa\lambda}^{(\mathbb{P}f_{2\mathbb{R}}M)}(q_1, q_2)|_{\text{bare}}$  and  $\Gamma_{\mu\nu,\kappa\lambda}^{(\mathbb{P}f_{2\mathbb{R}}M)}(q_1, q_2)|_{\text{bare}}$ , respectively. The results are as in (2.18) and (2.19) but with the replacements

$$\begin{aligned} g'_{\mathbb{P}PM} &\rightarrow g'_{\mathbb{P}f_{2\mathbb{R}}M}, \\ g''_{\mathbb{P}PM} &\rightarrow g''_{\mathbb{P}f_{2\mathbb{R}}M}. \end{aligned} \quad (\text{A6})$$

This concludes our discussion of the  $\mathbb{P}f_{2\mathbb{R}}M$  couplings.

- 
- [1] P. Lebiedowicz, O. Nachtmann, and A. Szczurek, *Exclusive central diffractive production of scalar and pseudoscalar mesons; tensorial vs. vectorial pomeron*, Annals Phys. **344** (2014) 301, arXiv:1309.3913 [hep-ph].
- [2] C. Ewerz, M. Maniatis, and O. Nachtmann, *A Model for Soft High-Energy Scattering: Tensor Pomeron and Vector Odderon*, Annals Phys. **342** (2014) 31, arXiv:1309.3478 [hep-ph].
- [3] D. Barberis *et al.*, (WA102 Collaboration), *A study of pseudoscalar states produced centrally in pp interactions at 450 GeV/c*, Phys. Lett. **B427** (1998) 398, arXiv:hep-ex/9803029.
- [4] A. Kirk, *Resonance production in central pp collisions at the CERN Omega spectrometer*, Phys. Lett. B **489** (2000) 29, arXiv:hep-ph/0008053.
- [5] P. Lebiedowicz, J. Leutgeb, O. Nachtmann, A. Rebhan, and A. Szczurek, *Central exclusive diffractive production of axial-vector  $f_1(1285)$  and  $f_1(1420)$  mesons in proton-proton collisions*, Phys. Rev. D **102** no. 11, (2020) 114003, arXiv:2008.07452 [hep-ph].

- [6] N. I. Kochelev, T. Morii, and A. V. Vinnikov, *Pomeron fusion and central  $\eta$  and  $\eta'$  meson production*, Phys.Lett. **B457** (1999) 202, arXiv:hep-ph/9903279 [hep-ph].
- [7] N. I. Kochelev, T. Morii, B. L. Reznik, and A. V. Vinnikov, *The role of secondary Reggeons in central meson production*, Eur.Phys.J. **A8** (2000) 405, arXiv:hep-ph/0005088 [hep-ph].
- [8] E. Shuryak and I. Zahed, *Semiclassical double pomeron production of glueballs and  $\eta'$* , Phys.Rev. **D68** (2003) 034001, arXiv:hep-ph/0302231 [hep-ph].
- [9] V. A. Petrov, R. A. Ryutin, A. E. Sobol, and J.-P. Guillaud, *Azimuthal angular distributions in EDDE as spin-parity analyser and glueball filter for LHC*, JHEP **0506** (2005) 007, arXiv:hep-ph/0409118 [hep-ph].
- [10] R. A. Ryutin, *Visualizations of exclusive central diffraction*, Eur. Phys. J. C **74** no. 11, (2014) 3162, arXiv:1404.7678 [hep-ph].
- [11] C. Ewerz, P. Lebiedowicz, O. Nachtmann, and A. Szczurek, *Helicity in Proton-Proton Elastic Scattering and the Spin Structure of the Pomeron*, Phys. Lett. **B763** (2016) 382, arXiv:1606.08067 [hep-ph].
- [12] L. Adamczyk *et al.*, (STAR Collaboration), *Single spin asymmetry  $A_N$  in polarized proton-proton elastic scattering at  $\sqrt{s} = 200$  GeV*, Phys. Lett. **B719** (2013) 62, arXiv:1206.1928 [nucl-ex].
- [13] D. Britzger, C. Ewerz, S. Glazov, O. Nachtmann, and S. Schmitt, *Tensor Pomeron and low-x deep inelastic scattering*, Phys. Rev. **D100** no. 11, (2019) 114007, arXiv:1901.08524 [hep-ph].
- [14] F. E. Close and G. A. Schuler, *Central production of mesons: Exotic states versus pomeron structure*, Phys.Lett. **B458** (1999) 127, arXiv:hep-ph/9902243 [hep-ph].
- [15] F. E. Close and G. A. Schuler, *Evidence that the Pomeron transforms as a non-conserved vector current*, Phys.Lett. **B464** (1999) 279, arXiv:hep-ph/9905305 [hep-ph].
- [16] D. Barberis *et al.*, (WA102 Collaboration), *Experimental evidence for a vector like behavior of Pomeron exchange*, Phys. Lett. **B467** (1999) 165, arXiv:hep-ex/9909013.
- [17] P. Lebiedowicz, O. Nachtmann, and A. Szczurek, *Central exclusive diffractive production of the  $\pi^+\pi^-$  continuum, scalar, and tensor resonances in  $pp$  and  $p\bar{p}$  scattering within the tensor Pomeron approach*, Phys. Rev. **D93** (2016) 054015, arXiv:1601.04537 [hep-ph].
- [18] P. Lebiedowicz, O. Nachtmann, and A. Szczurek, *Towards a complete study of central exclusive production of  $K^+K^-$  pairs in proton-proton collisions within the tensor Pomeron approach*, Phys. Rev. **D98** (2018) 014001, arXiv:1804.04706 [hep-ph].
- [19] P. Lebiedowicz, O. Nachtmann, and A. Szczurek, *Central exclusive diffractive production of  $K^+K^-K^+K^-$  via the intermediate  $\phi\phi$  state in proton-proton collisions*, Phys. Rev. **D99** no. 9, (2019) 094034, arXiv:1901.11490 [hep-ph].
- [20] P. Lebiedowicz, O. Nachtmann, and A. Szczurek, *Extracting the Pomeron-Pomeron- $f_2(1270)$  coupling in the  $pp \rightarrow pp\pi^+\pi^-$  reaction through the angular distribution of the pions*, Phys. Rev. **D101** no. 3, (2020) 034008, arXiv:1901.07788 [hep-ph].
- [21] P. Lebiedowicz, O. Nachtmann, and A. Szczurek, *Searching for the odderon in  $pp \rightarrow ppK^+K^-$  and  $pp \rightarrow pp\mu^+\mu^-$  reactions in the  $\phi(1020)$  resonance region at the LHC*, Phys. Rev. D **101** (2020) 094012, arXiv:1911.01909 [hep-ph].
- [22] P. Lebiedowicz, *Study of the exclusive reaction  $pp \rightarrow ppK^{*0}\bar{K}^{*0}$ :  $f_2(1950)$  resonance versus diffractive continuum*, Phys. Rev. D **103** no. 5, (2021) 054039, arXiv:2102.13029 [hep-ph].
- [23] M. J. Anderson, S. K. Domokos, J. A. Harvey, and N. Mann, *Central production of  $\eta$  and  $\eta'$  via double Pomeron exchange in the Sakai-Sugimoto model*, Phys. Rev. **D90** no. 8, (2014) 086010, arXiv:1406.7010 [hep-ph].
- [24] M. J. Anderson, S. Domokos, and N. Mann, *Central production of  $\eta$  via double Pomeron exchange and double Reggeon exchange in the Sakai-Sugimoto model*, Phys. Rev. D **96** no. 4, (2017) 046002, arXiv:1612.07457 [hep-ph].
- [25] F. Hechenberger, Thesis, *Central Exclusive Production of Pseudoscalar and Axial Vector Mesons through Pomeron Fusion*, Technische Universität Wien, 2020. <https://repositum.tuwien.ac.at/urn:nbn:at:at-ubtuw:1-134144>.
- [26] A. Szczurek, R. S. Pasechnik, and O. V. Teryaev,  *$pp \rightarrow pp\eta'$  reaction at high energies*, Phys.Rev. **D75** (2007) 054021, arXiv:hep-ph/0608302 [hep-ph].
- [27] L. A. Harland-Lang, V. A. Khoze, M. G. Ryskin, and W. J. Stirling, *Central exclusive production as a probe of the gluonic component of the  $\eta'$  and  $\eta$  mesons*, Eur. Phys. J. C **73** (2013) 2429, arXiv:1302.2004 [hep-ph].
- [28] P. D. B. Collins, *An Introduction to Regge Theory and High-Energy Physics*. Cambridge University Press, Cambridge, England, 1977.
- [29] F. E. Close and A. Kirk, *Glueball -  $q\bar{q}$  filter in central hadron production*, Phys.Lett. **B397** (1997) 333, arXiv:hep-ph/9701222 [hep-ph].
- [30] D. Barberis *et al.*, (WA102 Collaboration), *A kinematical selection of glueball candidates in central production*, Phys.Lett. **B397** (1997) 339.
- [31] S. Navas *et al.*, (Particle Data Group), *Review of particle physics*, Phys. Rev. D **110** no. 3, (2024) 030001.
- [32] A. Cisek, P. Lebiedowicz, W. Schäfer, and A. Szczurek, *Exclusive production of  $\omega$  meson in proton-proton collisions at high energies*, Phys.Rev. **D83** (2011) 114004, arXiv:1101.4874 [hep-ph].
- [33] M. Diehl, P. Kroll, and C. Vogt, *The annihilation of virtual photons into pseudoscalar mesons*, Eur. Phys. J. C **22** (2001) 439, arXiv:hep-ph/0108220.
- [34] P. Kroll and K. Passek-Kumerički, *Two gluon components of the  $\eta$  and  $\eta'$  mesons to leading-twist accuracy*, Phys.Rev. **D67** (2003) 054017, arXiv:hep-ph/0210045 [hep-ph].
- [35] P. Kroll and K. Passek-Kumerički, *Wide-angle photoproduction of the  $\eta'$ -meson and its gluon content*, Phys. Rev. D **105** no. 3, (2022) 034005, arXiv:2111.08965 [hep-ph].
- [36] A. Donnachie, H. G. Dosch, P. V. Landshoff, and O. Nachtmann, *Pomeron physics and QCD*, Camb. Monogr. Part. Phys., Nucl. Phys., Cosmol. **19** (2002) 1.
- [37] O. Nachtmann, *Considerations concerning diffraction scattering in quantum chromodynamics*, Annals Phys. **209** (1991) 436.
- [38] O. Nachtmann, *High Energy Collisions and Nonperturbative QCD in "Perturbative and Nonperturbative Aspects of Quantum*



Field Theory", H. Latal, W. Schweiger (Eds.), Springer-Verlag, Berlin, Heidelberg (1997), published in: Lect. Notes Phys. 479 (1997) 49-138, <https://doi.org/10.1007/BFb0104289>.